

Quantum semi-supervised generative adversarial network for enhanced data classification

Kouhei Nakaji and Naoki Yamamoto

Department of Applied Physics and Physico-Informatics & Quantum Computing Center, Keio University, Hiyoshi 3-14-1, Kohoku, Yokohama, 223-8522, Japan

February 4, 2022

Abstract

In this paper, we propose the quantum semi-supervised generative adversarial network (qSGAN). The system is composed of a quantum generator and a classical discriminator/classifier (D/C). The goal is to train both the generator and the D/C, so that the latter may get a high classification accuracy for a given dataset. The generator needs neither any data loading nor to generate a pure quantum state, while it is expected to serve as a stronger adversary than a classical one thanks to its rich expressibility. These advantages are demonstrated in a numerical simulation.

1 Introduction

We are witnessing active challenges to develop several type of enhanced machine learning schemes via quantum computing, i.e., the research field of quantum machine learning [1–7]. In particular, based on the possible higher expressibility of quantum circuits over the classical one, which has been proven theoretically and demonstrated experimentally [8–12], the quantum machine learning is expected to provide alternative subroutines to improve the performance. For instance, the quantum classifier [3,4,6,7] is a quantum circuit that may be able to classify the input classical data with higher classification accuracy than conventional classical schemes such as the support vector machine. Note that many of those quantum machine learning applications need additional quantum operations or QRAM [13] to load the classical data into the quantum circuit, which eventually may vanish the possible quantum advantage.

The machine learning scheme focused in this paper is the generative adversarial network (GAN) [14]. In general, GAN consists of two adversarial components, typically a generator (generating a fake data) and a discriminator (discriminating a real or fake data), and their adversarial training yields an outperforming system over the one trained solely. GAN is also a topic actively studied in the quantum machine learning regime [15–29]. For example, Refs. [15,16] provide a method to train the quantum generative model by using GAN, where both the discriminator and the generator are quantum systems. Also [17] pro-

vides a method to synthesize a quantum generative model for discrete dataset, in the GAN framework. A useful application of GAN was proposed in [18]; their GAN consists of a quantum generator and a classical discriminator, and via the adversarial training the generator acquires the quantum state corresponding to a target probability distribution, which is then sent to another quantum circuit running a Grover-type algorithm (more precisely, the amplitude estimation algorithm for Monte Carlo simulation). Note that, however, this means that the generator is required to produce a target pure quantum state.

In this paper, we propose the *quantum semi-supervised GAN (qSGAN)*. As in the case of standard GAN, the SGAN [30–33] consists of a generator and a discriminator, but the role of discriminator is to discriminate real/fake of the input data plus to estimate its label; that is, the goal of SGAN is to train the discriminator so that it becomes a good classifier, rather than realizing a high-quality generator. Our qSGAN consists of a quantum generator and a classical discriminator, like the case of [18], but the main goal is to train the classical discriminator rather than the quantum generator. In other words, the quantum system is used to train the classical system. Therefore, our qSGAN needs neither any data loading nor to generate a pure quantum state, while it is expected to serve as a stronger adversary than a classical one, based on its rich expressibility.

The rest of the paper is organized as follows. Section 2 is devoted to provide the algorithm of qSGAN. Section 3 gives a numerical simulation to demonstrate the performance of qSGAN, with particular focus on the size of quantum circuit and the number of labeled training data. Also we show the expected noise-tolerant property of qSGAN. Moreover, we compare the quantum generator to a classical (deep) neural network generator and show that the resulting classification performance are comparable in a specific condition, suggesting a possible advantage of qSGAN for classification problems. Finally in Section 4, we conclude the paper.

2 Algorithm of qSGAN

First let us recall the idea of standard GAN. GAN consists of a generator and a discriminator. The generator

transforms a set of random seeds to samples (fake data). The discriminator receives either a real data from the data source or a fake data from the generator. Then the discriminator is trained so that it correctly classifies the received data into real or fake exclusively. Also the generator is trained so that its output (i.e., the fake data) are classified into real by the discriminator. Namely, the generator tries to fool the discriminator, and the discriminator tries to detect whether the received data is fake or real. If the training is successfully finished, then the generator acquires the ability to produce samples governed by a probability distribution that resembles the original distribution producing the real data. In what follows, we describe the algorithm of qSGAN, based on the original proposal [32].

(Source of the real data) Suppose that we have N_B data batches, and each batch contains ℓ labeled and $m - \ell$ unlabeled data. We write the set of labeled data in the a -th batch as $\{(\mathbf{x}_L^{a,1}, y^{a,1}), (\mathbf{x}_L^{a,2}, y^{a,2}), \dots, (\mathbf{x}_L^{a,\ell}, y^{a,\ell})\}$ and that of unlabeled data as $\{\mathbf{x}_{UL}^{a,1}, \mathbf{x}_{UL}^{a,2}, \dots, \mathbf{x}_{UL}^{a,m-\ell}\}$, where $y^{a,i}$ is the label of the i -th labeled data in the a -th batch. We summarize \mathbf{x}_L and \mathbf{x}_{UL} into a single data vector as

$$\mathbf{x}_{\text{data}}^{a,i} = \begin{cases} \mathbf{x}_L^{a,i} & i \leq \ell \\ \mathbf{x}_{UL}^{a,i-\ell} & \text{otherwise} \end{cases}. \quad (1)$$

The label data $y^{a,i}$ takes one of the values of $\{1, \dots, c\}$, where c is the number of classes.

(Generator) The generator is a quantum circuit composed of qubits, which prepares the quantum state $|\psi\rangle = U(\boldsymbol{\theta})|0\rangle$, where $|0\rangle$ denotes the initial state of the circuit and $U(\boldsymbol{\theta})$ is the unitary matrix corresponding to the parametrized quantum circuit with parameters $\boldsymbol{\theta}$. The circuit outputs a fake data \mathbf{x}_{fake} as a result of the measurement of $|\psi\rangle$ in the computational basis. That is, \mathbf{x}_{fake} appears with probability $\mathbf{P}(\mathbf{x}_{\text{fake}}) = |\langle \mathbf{x}_{\text{fake}} | U(\boldsymbol{\theta}) | 0 \rangle|^2$. Note that the stochasticity of the generator comes from this quantum intrinsic property, rather than the added random seeds like the classical GAN.

(Discriminator/Classifier) In the SGAN framework, the discriminator $D(\mathbf{x})$, which judges real or fake for the received data \mathbf{x} , has an additional function, the label classifier $C(\mathbf{x})$. Hence, following Ref. [32], we call this classical system simply the D/C. More precise description of those functions is as follows. First, $D(\mathbf{x})$ represents the likelihood that the received \mathbf{x} came from the real data source. Next, $C(\mathbf{x})$ is a vector whose dimension is $c + 1$; the i -th ($1 \leq i \leq c$) component represents the likelihood that \mathbf{x} belongs to i -th class, and the last one is the likelihood that \mathbf{x} is a fake data. In this paper, we use a double-headed classical neural network to implement $C(\mathbf{x})$ and $D(\mathbf{x})$;

$$C(\mathbf{x}) = g(f(\mathbf{x})), \quad D(\mathbf{x}) = k(f(\mathbf{x})). \quad (2)$$

f is the function of the network shared by both $C(\mathbf{x})$ and $D(\mathbf{x})$, while g and k are the functions corresponding to the final layer; see Figure 3.

(Training rule) In the training process in each batch, m real data are loaded from the data source, and m fake data are generated by the generator, which are sent to the D/C. Then the D/C assigns a label to those data via

$C(\mathbf{x})$ and also judges real/fake via $D(\mathbf{x})$. Based on those results, the parameters of the generator and the D/C are updated, according to the following rule.

First, the generator is updated so that the generated fake data are classified into real by the discriminator. More specifically, we minimize the following cost function L_G to update the parameters $\boldsymbol{\theta}$:

$$\begin{aligned} L_G &= \mathbf{E}_{\mathbf{x} \sim \text{Generator}} (-\log D(\mathbf{x})) \\ &= \sum_{\mathbf{x}} (-\log D(\mathbf{x})) |\langle \mathbf{x} | U(\boldsymbol{\theta}) | 0 \rangle|^2 \\ &\simeq -\frac{1}{m} \sum_{i=1}^m \log(D(\mathbf{x}_{\text{fake}}^i)), \end{aligned} \quad (3)$$

where $\mathbf{x}_{\text{fake}}^i$ is the i -th fake sample. Roughly speaking, minimizing L_G corresponds to maximizing $D(\mathbf{x}_{\text{fake}}^i)$, i.e., the likelihood that the fake data came from the real data source. In this paper, we take a quantum circuit where each parameter element θ_q is embedded into a single qubit gate in the form $U_q = \exp(-i\theta_q A_q/2)$ with A_q the single qubit operator satisfying $A_q^2 = \mathbf{1}$. In this case, the gradient of L_G is calculated as follows [34]:

$$\begin{aligned} \frac{\partial L_G}{\partial \theta_q} &= \frac{1}{2} \sum_{\mathbf{x}} (-\log D(\mathbf{x})) \left(|\langle \mathbf{x} | U_{q+}(\boldsymbol{\theta}) | 0 \rangle|^2 \right. \\ &\quad \left. - |\langle \mathbf{x} | U_{q-}(\boldsymbol{\theta}) | 0 \rangle|^2 \right), \end{aligned} \quad (4)$$

where

$$\begin{aligned} U_{q\pm}(\boldsymbol{\theta}) &= U_{q\pm}(\{\theta_1, \dots, \theta_{q-1}, \theta_q, \theta_{q+1}, \dots, \theta_n\}) \\ &= U(\{\theta_1, \dots, \theta_{q-1}, \theta_q \pm \pi/2, \theta_{q+1}, \dots, \theta_n\}). \end{aligned} \quad (5)$$

Thus, given the fake data $\mathbf{x}_{\text{fake}}^{(q\pm)i}$ obtained by measuring $U_{q\pm}(\boldsymbol{\theta})|0\rangle$, we get an unbiased estimator of $\partial L_G / \partial \theta_q$ as

$$\frac{\partial L_G}{\partial \theta_q} \simeq \frac{1}{2m} \sum_{i=1}^m \left[-\log D(\mathbf{x}_{\text{fake}}^{(q+)i}) + \log D(\mathbf{x}_{\text{fake}}^{(q-)i}) \right]. \quad (6)$$

This gradient descent vector is used to construct an optimizer for minimizing L_G .

Second, the D/C is trained so that it makes a correct real/fake judgement on the received data by $D(\mathbf{x})$ and, in addition, classifies them into the true class by $C(\mathbf{x})$. Hence, the parameters of the classical neural network are updated by minimizing the following cost function $L_{D/C}$:

$$\begin{aligned} L_{D/C} &= (L_D + L_C)/2, \\ L_D &= \mathbf{E}_{\mathbf{x} \sim \text{Generator}} [-\log(1 - D(\mathbf{x}))] \\ &\quad + \mathbf{E}_{\mathbf{x} \sim \text{Source}} [-\log(D(\mathbf{x}))] \\ &\simeq -\frac{1}{m} \sum_{i=1}^m \left(\log(1 - D(\mathbf{x}_{\text{fake}}^i)) + \log D(\mathbf{x}_{\text{data}}^{a,i}) \right), \\ L_C &= \mathbf{E}_{\mathbf{x} \sim \text{Generator}} [h(c+1, C(\mathbf{x}))] \\ &\quad + \mathbf{E}_{\mathbf{x} \sim \text{Labeled Source}} [h(y^i, C(\mathbf{x}))] \\ &\simeq \frac{1}{m} \sum_{i=1}^m h(c+1, C(\mathbf{x}_{\text{fake}}^i)) + \frac{1}{\ell} \sum_{i=1}^{\ell} h(y^i, C(\mathbf{x}_L^{a,i})). \end{aligned} \quad (7)$$

Algorithm 1 qSGAN

```
1: for  $j = 1$  to  $N_{\text{iter}}$  do
2:   for  $a = 1$  to  $N_B$  do
3:     Load labeled data  $\{(\mathbf{x}_L^{a,1}, y^{a,1}), (\mathbf{x}_L^{a,2}, y^{a,2}), \dots, (\mathbf{x}_L^{a,\ell}, y^{a,\ell})\}$  and unlabeled data as  $\{\mathbf{x}_{\text{UL}}^{a,1}, \mathbf{x}_{\text{UL}}^{a,2}, \dots, \mathbf{x}_{\text{UL}}^{a,m-\ell}\}$ .
4:     for  $i = 1$  to  $m$  do
5:       Set  $\mathbf{x}_{\text{fake}}^i$  to the measurement result of  $|\psi\rangle = U(\boldsymbol{\theta})|0\rangle$ .
6:     end for
7:     for  $q = 1$  to  $n$  do
8:       for  $i = 1$  to  $m$  do
9:         Set  $\mathbf{x}_{\text{fake}}^{q(+),i}$  to the measurement result of  $|\psi\rangle = U_{q+}(\boldsymbol{\theta})|0\rangle$ .
10:        Set  $\mathbf{x}_{\text{fake}}^{q(-),i}$  to the measurement result of  $|\psi\rangle = U_{q-}(\boldsymbol{\theta})|0\rangle$ .
11:      end for
12:      Set  $\frac{\partial L_G}{\partial \theta_q}$  to  $\frac{1}{2m} \sum_{i=1}^m \left[ -\log D(\mathbf{x}_{\text{fake}}^{q(+),i}) + \log D(\mathbf{x}_{\text{fake}}^{q(-),i}) \right]$ .
13:    end for
14:    Update  $\boldsymbol{\theta}$  by the gradient descent algorithm using  $\frac{\partial L_G}{\partial \theta_q}$  ( $q = 1, 2, \dots, n$ ).
15:    Set  $L_D$  to  $-\frac{1}{m} \sum_{i=1}^m \left[ \log(1 - D(\mathbf{x}_{\text{fake}}^i)) + \log D(\mathbf{x}_{\text{data}}^i) \right]$ .
16:    Set  $L_C$  to  $\frac{1}{m} \sum_{i=1}^m h(c+1, C(\mathbf{x}_{\text{fake}}^i)) + \frac{1}{\ell} \sum_{i=1}^{\ell} h(y^{a,i}, C(\mathbf{x}_L^{a,i}))$ .
17:    Set  $L_{D/C}$  to  $(L_D + L_C)/2$ .
18:    Compute the gradients of  $C(\mathbf{x})$  and  $D(\mathbf{x})$  by the back-propagation using  $L_{D/C}$  and update the parameters
    by the gradient descent algorithm.
19:  end for
20: end for
21: The Classifier  $C(\mathbf{x})$  as the final result
```

Here $h(y, \mathbf{z})$ is the cross entropy of the discrete distribution $q(i) = \exp(z_i) / (\sum_{j=1}^d \exp(z_j))$ ($i = 1, 2, \dots, d$) relative to the distribution $p(i) = \delta_{iy}$, defined as

$$h(y, \mathbf{z}) = -z_y + \log \left(\sum_{j=1}^d \exp(z_j) \right), \quad (8)$$

where z_j is the j -th element of the vector \mathbf{z} and d is the dimension of \mathbf{z} . As in the case of the generator, we use the gradient descent vector of $L_{D/C}$ to update the neural network parameters. In each iteration, the parameters are updated for all the batches. At the end of the training process with sufficiently large number of iterations, the trained D/C is obtained. The overall algorithm is summarized in Algorithm 1 with N_{iter} as the number of iteration.

3 Numerical demonstration

In this section, we demonstrate the performance of the proposed qSGAN method by a numerical simulation. In particular, we will see that a quantum generator with higher expressibility leads to a better classifier, after successful training. Also the resulting classification accuracy is comparable to that achieved when using a standard classical neural network generator.

Problem setting and result

The source of real data used in this simulation is a set of 1×8 pixel images, shown in Figure 1. Each pixel takes the value of 0 (black) or 1 (white). Also the label ‘0’ or ‘1’ is assigned to each image (hence $c = 2$) according to the following rule; if white pixels in an image are all

connected or there is only one white pixel in an image, then that image is labeled as ‘0’; If white pixels in an image are separated into two disconnected parts, then the image is labeled as ‘1’. The number of images with label ‘0’ and those with label ‘1’ are both 28 (hence 56 images in total). The dataset is separated into eight batches, each containing $m = 7$ images.

As the quantum generator, we use a 8-qubits parametrized quantum circuit with single layer or four layers; the case of four layers is shown in Figure 2. Each layer is composed of parametrized single-qubit rotational gates $\exp(-i\theta_i \sigma_{a_i}/2)$ and CNOT gates that connect adjacent qubits; here θ_i is the i -th parameter and σ_{a_i} is the Pauli operator ($a_i = x, y, z$). We randomly initialize all θ_i and a_i at the beginning of each training. We run the numerical simulation on Qiskit QASM Simulator [35].

As the D/C, we use a neural network with four layers, shown in Figure 3. The first three layers are shared by both the discriminator $D(\mathbf{x})$ and the classifier $C(\mathbf{x})$. The number of nodes in the first, second, and third layer are 8, 56, and 8, respectively; all nodes between the layers are fully connected, and we use ReLU as the activation functions. The last layer for the classifier has three nodes, corresponding to the likelihood of label ‘0’, label ‘1’, and fake classes; these nodes are fully connected to those of the third layer, and the softmax function is used as the activation function. The last layer of the discriminator has one node, simply giving the value of $D(\mathbf{x})$; this node is fully connected to the nodes of the third layer, and the sigmoid function ($\sigma(x) = 1/(1 + \exp(-x))$) is used as the activation function. We implement the neural networks by PyTorch [36].

In each trial of the algorithm, we choose two of the eight batches as the training dataset (hence $N_B = 2$) and the

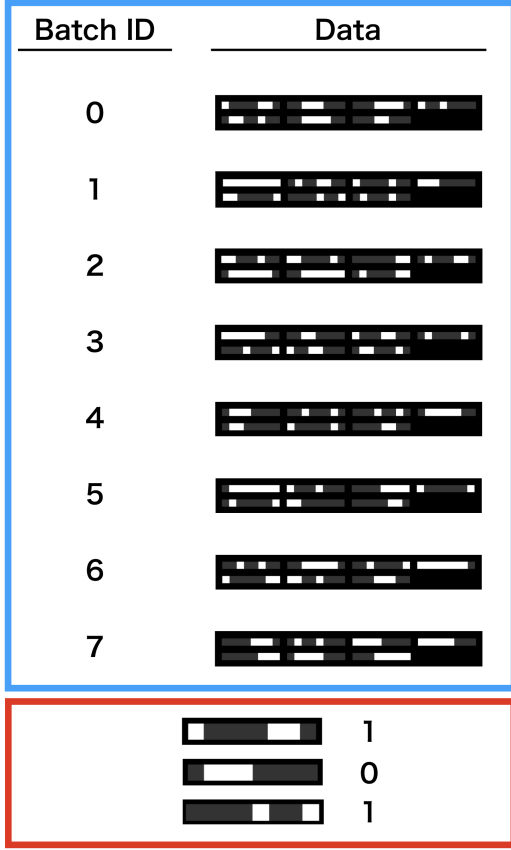


Figure 1: Top (enclosed by the blue rectangular): The dataset (= four batches) used in the numerical simulation. Bottom (enclosed by the red rectangular): Examples of images and their labels.

Training Data (Batch ID)	Test Data (Batch ID)	# of Trials
0,1	2,3,4,5,6,7	20
2,3	0,1,4,5,6,7	20
4,5	0,1,2,3,6,7	20
6,7	0,1,2,3,4,5	20

Table 1: The combination of the training/test dataset for the 4-fold cross validation.

other six as the test dataset. We perform the 4-fold cross validation by changing the training and test dataset, as summarized in Table 1. For each training/test dataset, we execute 20 trials (80 trials totally). To demonstrate the semi-supervised learning, some of the labels in each batch are masked; recall that the number of labeled example in each batch is denoted by ℓ , which takes $\ell = 2$ or 5 in this simulation. As the gradient descent algorithm, we use Adam [37], whose learning coefficient is set to 0.001 for the case of generator and 0.005 for the case of D/C.

Figure 4 shows the average classification accuracy for the test data versus the number of iteration, which are obtained as the average over 80 trials. The two subfigures are obtained with different number of labeled data, as $\ell = 2$ and $\ell = 5$. In each subfigure, three cases are shown, depending on the type of generator; the quantum generator with one layer (blue) and that with four layer

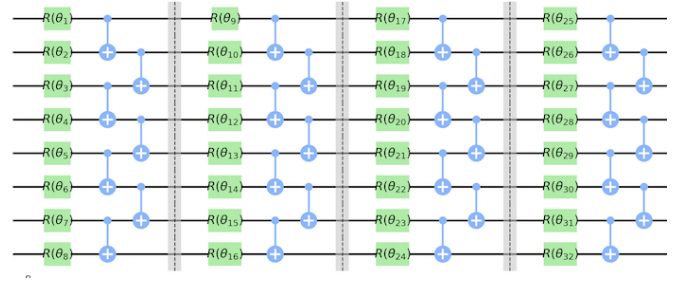


Figure 2: The quantum circuit with four layers used in the simulation.

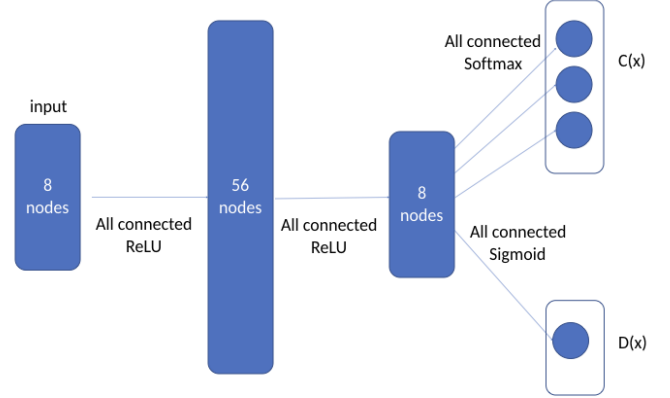


Figure 3: The D/C system, where the last layer functions as the classifier $C(x)$ or the discriminator $D(x)$.

(orange); also as a reference, the case of uniform-noise generator (green) that randomly generates 8-bit data with equal probability, which is not updated while training, is presented. The error bars represent the standard deviation of the average classification accuracy.

We see that, when only a few labeled data is available ($\ell = 2$), the quantum generator with four layers results in the highest classification accuracy, which implies that the quantum generator with bigger expressibility contributes to the higher accuracy by effectively generating samples to train the classical D/C. On the other hand, in the case where five of eight image data in each batch are labeled ($\ell = 5$), the three generators achieve almost the same accuracy. This might be because, in this case, all the generators fail to generate more valuable dataset than the set of labeled real data, for effectively training the D/C. This observation is supported by the fact that the untrained uniform-noise generator, which of course is not related to the real dataset, achieves almost the same classification accuracy. Therefore, we expect that the quantum generator is useful when the number of labeled data is limited.

In this numerical simulation, we obtained the best classification accuracy when the constructed classical sample distribution corresponding to the output of the quantum generator does not match the distribution producing the real dataset, as predicted in [38]. In addition, we found that the cost for the quantum generator, L_G , is larger than

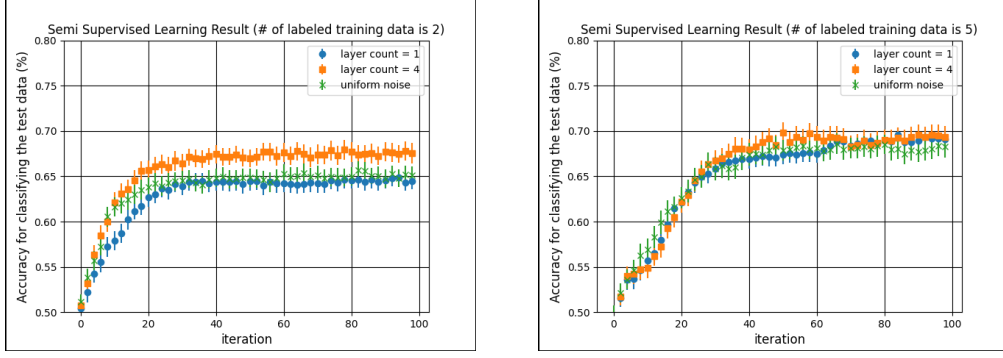


Figure 4: Classification accuracy of the classifier when using the quantum generator. The number of labeled data is $\ell = 2$ (left) and $\ell = 5$ (right).

that for the classical D/C, $L_{D/C}$, when the best accuracy is reached. These facts are favorable for the current noisy quantum devices that cannot be effectively trained due to the noise. In the next subsection we will see how much the noise affects on the quantum generator and accordingly the classification accuracy.

Noisy qSGAN

We examine the case where a noise channel is applied between the layers of the quantum generator. In particular we assume the depolarizing channel:

$$\mathcal{E}(\rho) = (1 - p)\rho + p\frac{I}{2^n}, \quad (9)$$

where ρ is a density matrix, I is the identity matrix, n is the number of qubits, and p is a noise parameter. Given the unitary operation $\mathcal{U}_i(\rho) = U_i\rho U_i^\dagger$ with the i -th depth unitary matrix U_i , the output density matrix is written as

$$\begin{aligned} \rho_{\text{out}} &= \mathcal{E} \circ \mathcal{U}_4 \circ \mathcal{E} \circ \mathcal{U}_3 \circ \mathcal{E} \circ \mathcal{U}_2 \circ \mathcal{E} \circ \mathcal{U}_1(|0\rangle\langle 0|) \\ &= \mathcal{E} \circ \mathcal{U}_4 \circ \mathcal{E} \circ \mathcal{U}_3 \circ \mathcal{E} \left((1 - p)U_2U_1|0\rangle\langle 0|U_1^\dagger U_2^\dagger + p\frac{I}{2^n} \right) \\ &= \dots \\ &= (1 - p)^4 U_4U_3U_2U_1|0\rangle\langle 0|U_1^\dagger U_2^\dagger U_3^\dagger U_4^\dagger \\ &\quad + (1 - (1 - p)^4) \frac{I}{2^n}. \end{aligned} \quad (10)$$

The samples are generated by measuring ρ_{out} . Other than the presence of noise, the simulation setting are the same as the noiseless case. We examine the case when only a few labeled data is available ($\ell = 2$).

The resulting classification accuracy achieved via the quantum generator under the depolarization noise is shown in Figure 5, with several values of noise strength p . The horizontal axis represents the magnitude of total noise, i.e., the coefficient of the second term in Eq. (10), while the vertical axis represents the average classification accuracy at the final (= 100-th) iteration step. As in Figure 4, the error bar is the standard deviation of the average accuracy. The result is that, as discussed at the bottom of previous subsection, the classification accuracy does not become worse than the noiseless case, as long

as the depolarization noise for each layer of the quantum generator is suppressed to some level ($p = 0.05$). This demonstrates the second advantage of the proposed qSGAN described in Section 1; that is, the quantum generator in our qSGAN framework does not need to generate a pure quantum state.

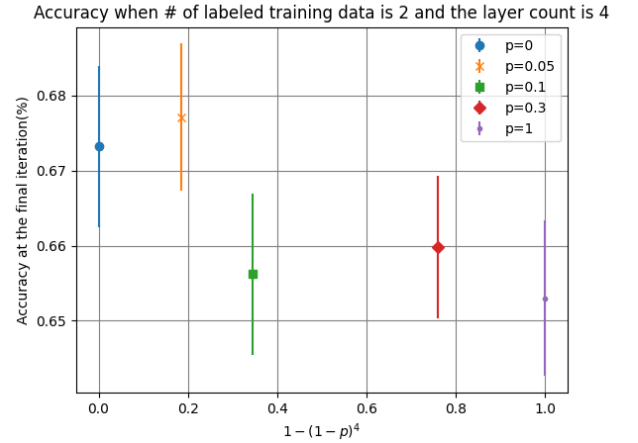


Figure 5: Classification accuracy of the classifier for $\ell = 2$ when using the four-layers quantum generator under the depolarization noise (9).

Comparison with a classical neural network generator

Finally, we compare the performance of the proposed qSGAN to the fully classical case where the generator is served by a five-layers classical neural network. The structure of this neural network is shown in Figure 6. The input to the network is the 1-dimensional normal Gaussian noise with zero mean and unit variance. The second, third, and fourth layer are composed of 40 nodes, and the fifth (= final) layer has 8 nodes. The nodes between the layers are fully connected and ReLU is used as the activation function. The output sample is obtained by transforming the values of the nodes at the final layer by the sigmoid

function ($\sigma(x) = 1/(1+e^{-x})$). We use the same D/C used in the quantum case. As the gradient descent algorithm, we use Adam, whose learning coefficients are set to 0.001 for both the generator and the D/C. Figure 7 shows the classification accuracy for the test data over the number of iteration, which are obtained as the average over 80 trials when using the classical neural network generator. As in the case of Figure 4, the two subfigures are obtained with different number of labeled data, as $\ell = 2$ and $\ell = 5$.

The result is that, for the case $\ell = 2$, the classifier aided by the classical neural network generator achieves the classification accuracy about 67%, which is comparable to that of the four-layers quantum generator. The notable point is that the number of parameters of the classical and quantum generators are 3688 and 32, respectively. Hence, naively, the quantum generator has a rich expressibility power comparable to the classical one even with much fewer parameters. This means that the training of the quantum generator is easier than the classical one, which is actually shown in Figures 4 and 7; about 40 iterations is enough to reach the accuracy 67% for the former case, while the latter requires roughly 400 iterations to reach the same accuracy. More importantly, this result implies that a bigger quantum generator with tractable number of parameters could have a potential to work even for some problems that are intractable via any classical one due to the explosion of the number of parameters.

4 Conclusion

In this paper, we provided qSGAN that performs a semi-supervised learning task by GAN composed of the quantum generator and the classical discriminator/classifier. This system has the following clear merits. That is, it needs neither data loading nor to generate a pure quantum state; rather its main role is to train the classical classifier, as a possibly stronger adversary than a classical one. The numerical experiment using the connected-disconnected image dataset shows that the rich expressibility of the quantum generator contributes to achieve the classification accuracy as high as that obtained when using the deep classical neural network generator (hence with much more parameters involved there). Also, we exemplified the noise-tolerant property of qSGAN under the depolarization noise, which is also a preferable feature for implementing qSGAN on a current noisy quantum device.

This work is supported by the MEXT Quantum Leap Flagship Program Grant Number JPMXS0118067285 and JPMXS0120319794.

References

- [1] Jacob Biamonte, Peter Wittek, Nicola Pancotti, Patrick Rebentrost, Nathan Wiebe, and Seth Lloyd. Quantum machine learning. *Nature*, 549(7671):195–202, 2017.
- [2] Siddharth Srinivasan, Carlton Downey, and Byron Boots. Learning and inference in hilbert space with quantum graphical models. In *Advances in Neural Information Processing Systems*, pages 10338–10347, 2018.
- [3] Maria Schuld, Ilya Sinayskiy, and Francesco Petruccione. Prediction by linear regression on a quantum computer. *Physical Review A*, 94(2):022342, 2016.
- [4] Vojtěch Havlíček, Antonio D Córcoles, Kristan Temme, Aram W Harrow, Abhinav Kandala, Jerry M Chow, and Jay M Gambetta. Supervised learning with quantum-enhanced feature spaces. *Nature*, 567(7747):209–212, 2019.
- [5] Carlo Ciliberto, Mark Herbster, Alessandro Davide Ialongo, Massimiliano Pontil, Andrea Rocchetto, Simone Severini, and Leonard Wossnig. Quantum machine learning: a classical perspective. *Proceedings of the Royal Society A: Mathematical, Physical and Engineering Sciences*, 474(2209):20170551, 2018.
- [6] Maria Schuld, Alex Bocharov, Krysta M Svore, and Nathan Wiebe. Circuit-centric quantum classifiers. *Physical Review A*, 101(3):032308, 2020.
- [7] Carsten Blank, Daniel K Park, June-Koo Kevin Rhee, and Francesco Petruccione. Quantum classifier with tailored quantum kernel. *npj Quantum Information*, 6(1):1–7, 2020.
- [8] Michael J Bremner, Richard Jozsa, and Dan J Shepherd. Classical simulation of commuting quantum computations implies collapse of the polynomial hierarchy. *Proceedings of the Royal Society A: Mathematical, Physical and Engineering Sciences*, 467(2126):459–472, 2011.
- [9] Michael J Bremner, Ashley Montanaro, and Dan J Shepherd. Average-case complexity versus approximate simulation of commuting quantum computations. *Physical Review Letters*, 117(8):080501, 2016.
- [10] Michael J Bremner, Ashley Montanaro, and Dan J Shepherd. Achieving quantum supremacy with sparse and noisy commuting quantum computations. *Quantum*, 1:8, 2017.
- [11] Edward Farhi and Aram W Harrow. Quantum supremacy through the quantum approximate optimization algorithm. *arXiv preprint arXiv:1602.07674*, 2016.
- [12] Frank Arute, Kunal Arya, Ryan Babbush, Dave Bacon, Joseph C Bardin, Rami Barends, Rupak Biswas, Sergio Boixo, Fernando G. S. L. Brandao, David A. Buell, Brian Burkett, Yu Chen, Zijun Chen, Ben Chiaro, Roberto Collins, William Courtney, Andrew Dunsworth, Edward Farhi, Brooks Foxen, Austin Fowler, Craig Gidney, Marissa Giustina, Rob Graff, Keith Guerin, Steve Habegger, Matthew P. Harrigan, Michael J. Hartmann, Alan Ho, Markus Hoffmann, Trent Huang, Travis S. Humble, Sergei V. Isakov, Evan Jeffrey, Zhang Jiang, Dvir Kafri, Kostyantyn Kechedzhi, Julian Kelly, Paul V. Klimov,

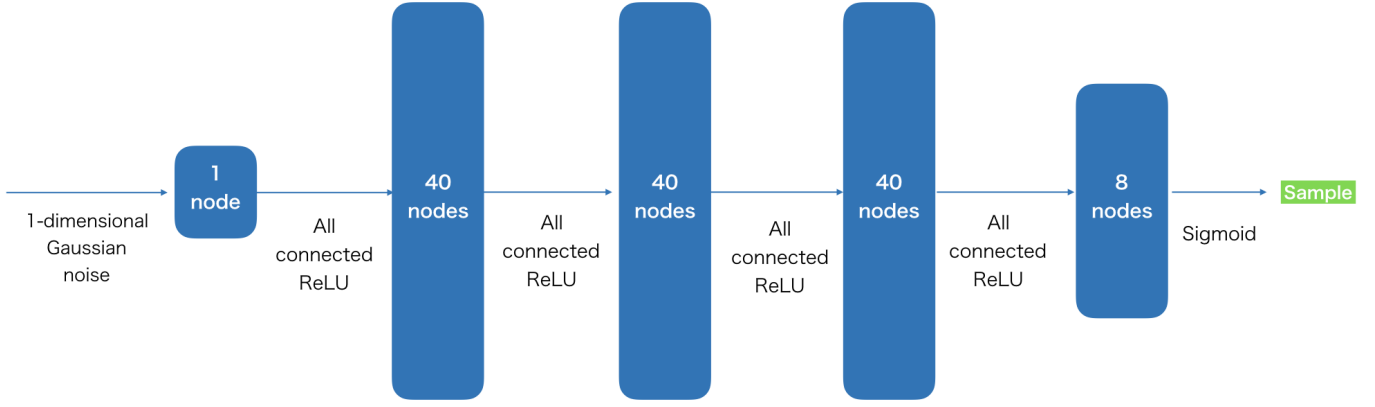


Figure 6: Structure of the classical neural network generator.

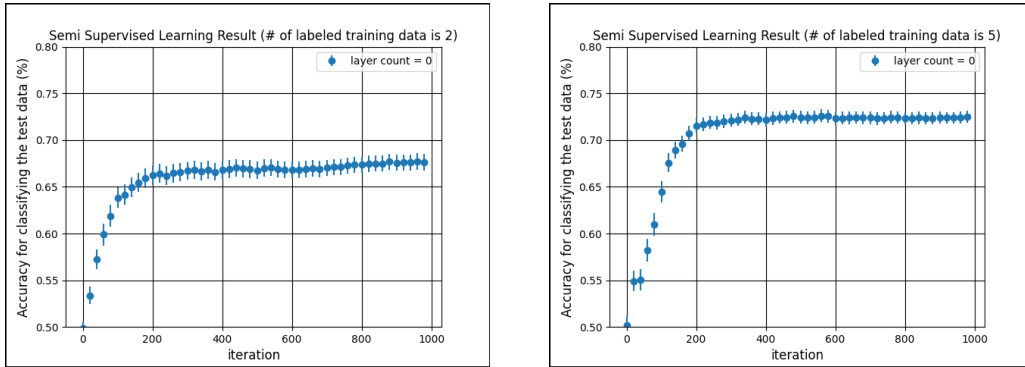


Figure 7: Classification accuracy of the classifier when using the five-layers classical neural network generator. The number of labeled data is $\ell = 2$ (left) and $\ell = 5$ (right).

- Sergey Knysh, Alexander Korotkov, Fedor Kostritsa, David Landhuis, Mike Lindmark, Erik Lucero, Dmitry Lyakh, Salvatore Mandrà, Jarrod R. McClean, Matthew McEwen, Anthony Megrant, Xiao Mi, Kristel Michielsen, Masoud Mohseni, Josh Mutus, Ofer Naaman, Matthew Neeley, Charles Neill, Murphy Yuezhen Niu, Eric Ostby, Andre Petukhov, John C. Platt, Chris Quintana, Eleanor G. Rieffel, Pedram Roushan, Nicholas C. Rubin, Daniel Sank, Kevin J. Satzinger, Vadim Smelyanskiy, Kevin J. Sung, Matthew D. Trevithick, Amit Vainsencher, Benjamin Villalonga, Theodore White, Z. Jamie Yao, Ping Yeh, Adam Zalcman, and Hartmut Neven & John M. Martinis. Quantum supremacy using a programmable superconducting processor. *Nature*, 574(7779):505–510, 2019.
- [13] Vittorio Giovannetti, Seth Lloyd, and Lorenzo Maccone. Quantum random access memory. *Physical Review Letters*, 100(16):160501, 2008.
- [14] Ian Goodfellow, Jean Pouget-Abadie, Mehdi Mirza, Bing Xu, David Warde-Farley, Sherjil Ozair, Aaron Courville, and Yoshua Bengio. Generative adversarial nets. In Z. Ghahramani, M. Welling, C. Cortes, N. D. Lawrence, and K. Q. Weinberger, editors, *Advances in Neural Information Processing Systems 27*, pages 2672–2680. Curran Associates, Inc., 2014.
- [15] Pierre-Luc Dallaire-Demers and Nathan Killoran. Quantum generative adversarial networks. *Physical Review A*, 98(1):012324, 2018.
- [16] Seth Lloyd and Christian Weedbrook. Quantum generative adversarial learning. *Physical Review Letters*, 121(4):040502, 2018.
- [17] Haozhen Situ, Zhimin He, Yuyi Wang, Lvzhou Li, and Shenggen Zheng. Quantum generative adversarial network for generating discrete distribution. *Information Sciences*, 538:193–208, 2020.
- [18] Christa Zoufal, Aurélien Lucchi, and Stefan Woerner. Quantum generative adversarial networks for learning and loading random distributions. *npj Quantum Information*, 5(1):1–9, 2019.
- [19] Marcello Benedetti, Edward Grant, Leonard Wossnig, and Simone Severini. Adversarial quantum circuit learning for pure state approximation. *New Journal of Physics*, 21(4):043023, 2019.

- [20] Ling Hu, Shu-Hao Wu, Weizhou Cai, Yuwei Ma, Xi-anghao Mu, Yuan Xu, Haiyan Wang, Yipu Song, Dong-Ling Deng, Chang-Ling Zou, and Luyan Sun. Quantum generative adversarial learning in a superconducting quantum circuit. *Science advances*, 5(1):eaav2761, 2019.
- [21] Jinfeng Zeng, Yufeng Wu, Jin-Guo Liu, Lei Wang, and Jiangping Hu. Learning and inference on generative adversarial quantum circuits. *Physical Review A*, 99(5):052306, 2019.
- [22] Jonathan Romero and Alan Aspuru-Guzik. Variational quantum generators: Generative adversarial quantum machine learning for continuous distributions. *arXiv preprint arXiv:1901.00848*, 2019.
- [23] Shouvanik Chakrabarti, Tongyang Yiming, Huang and Li, Soheil Feizi, and Xiaodi Wu. Quantum wasserstein generative adversarial networks. In *Advances in Neural Information Processing Systems*, pages 6781–6792, 2019.
- [24] Kaixuan Huang, Zheng-An Wang, Chao Song, Kai Xu, Hekang Li, Zhen Wang, Qiujiang Guo, Zixuan Song, Zhi-Bo Liu, Dongning Zheng, et al. Realizing a quantum generative adversarial network using a programmable superconducting processor. *arXiv preprint arXiv:2009.12827*, 2020.
- [25] He-Liang Huang, Yuxuan Du, Ming Gong, Youwei Zhao, Yulin Wu, Chaoyue Wang, Shaowei Li, Futian Liang, Jin Lin, Yu Xu, et al. Experimental quantum generative adversarial networks for image generation. *arXiv preprint arXiv:2010.06201*, 2020.
- [26] Abhinav Anand, Jonathan Romero, Matthias Degroote, and Alán Aspuru-Guzik. Experimental demonstration of a quantum generative adversarial network for continuous distributions. *arXiv preprint arXiv:2006.01976*, 2020.
- [27] Shahnawaz Ahmed, Carlos Sánchez Muñoz, Franco Nori, and Anton Frisk Kockum. Quantum state tomography with conditional generative adversarial networks. *arXiv preprint arXiv:2008.03240*, 2020.
- [28] Samuel A Stein, Betis Baheri, Ray Marie Tischio, Ying Mao, Qiang Guan, Ang Li, Bo Fang, and Shuai Xu. Qugan: A generative adversarial network through quantum states. *arXiv preprint arXiv:2010.09036*, 2020.
- [29] Daniel Herr, Benjamin Obert, and Matthias Rosenkranz. Anomaly detection with variational quantum generative adversarial networks. *arXiv preprint arXiv:2010.10492*, 2020.
- [30] Zhiyue Liu, Jiahai Wang, and Zhiwei Liang. Catgan: Category-aware generative adversarial networks with hierarchical evolutionary learning for category text generation. In *AAAI*, pages 8425–8432, 2020.
- [31] Tim Salimans, Ian Goodfellow, Wojciech Zaremba, Vicki Cheung, Alec Radford, and Xi Chen. Improved techniques for training gans. In *Advances in neural information processing systems*, pages 2234–2242, 2016.
- [32] Augustus Odena. Semi-supervised learning with generative adversarial networks. *arXiv preprint arXiv:1606.01583*, 2016.
- [33] Jie Gui, Zhenan Sun, Yonggang Wen, Dacheng Tao, and Jieping Ye. A review on generative adversarial networks: Algorithms, theory, and applications. *arXiv preprint arXiv:2001.06937*, 2020.
- [34] Jin-Guo Liu and Lei Wang. Differentiable learning of quantum circuit born machines. *Phys. Rev. A*, 98:062324, Dec 2018.
- [35] Héctor Abraham, AduOfiei, Rochisha Agarwal, Ismail Yunus Akhalwaya, Gadi Aleksandrowicz, Thomas Alexander, Matthew Amy, Eli Arbel, Arjit02, Abraham Asfaw, Artur Avkhadiiev, Carlos Azaustre, AzizNgoueya, Abhik Banerjee, Aman Bansal, Panagiotis Barkoutsos, George Barron, George S. Barron, Luciano Bello, Yael Ben-Haim, Daniel Bevenius, Arjun Bhohe, Lev S. Bishop, Carsten Blank, Sorin Bolos, Samuel Bosch, Brandon, Sergey Bravyi, Bryce-Fuller, David Bucher, Artemiy Burov, Fran Cabrera, Padraic Calpin, Lauren Capelluto, Jorge Carballo, Ginés Carrascal, Adrian Chen, Chun-Fu Chen, Edward Chen, Jielun (Chris) Chen, Richard Chen, Jerry M. Chow, Spencer Churchill, Christian Claus, Christian Clauss, Romilly Cocking, Filipe Correa, Abigail J. Cross, Andrew W. Cross, Simon Cross, Juan Cruz-Benito, Chris Culver, Antonio D. Córcoles-Gonzales, Sean Dague, Tareq El Dandachi, Marcus Daniels, Matthieu Dartiaill, DavideFrr, Abdón Rodríguez Davila, Anton Dekusar, Delton Ding, Jun Doi, Eric Drechsler, Drew, Eugene Dumitrescu, Karel Dumon, Ivan Duran, Kareem EL-Safty, Eric Eastman, Grant Eberle, Pieter Eendebak, Daniel Egger, Mark Everitt, Paco Martín Fernández, Axel Hernández Ferrera, Romain Fouilland, FranckChevallier, Albert Frisch, Andreas Fuhrer, Bryce Fuller, MELVIN GEORGE, Julien Gacon, Borja Godoy Gago, Claudio Gambella, Jay M. Gambetta, Adhisha Gammanpila, Luis Garcia, Tanya Garg, Shelly Garion, Austin Gilliam, Aditya Giridharan, Juan Gomez-Mosquera, Salvador de la Puente González, Jesse Gorzinski, Ian Gould, Donny Greenberg, Dmitry Grinko, Wen Guan, John A. Gunnels, Mikael Haglund, Isabel Haide, Ikko Hamamura, Omar Costa Hamido, Frank Harkins, Vojtech Havlicek, Joe Hellmers, Lukasz Herok, Stefan Hillmich, Hiroshi Horii, Connor Howington, Shaohan Hu, Wei Hu, Junye Huang, Rolf Huisman, Haruki Imai, Takashi Imamichi, Kazuaki Ishizaki, Raban Iten, Toshinari Itoko, JamesSeaward, Ali Javadi, Ali Javadi-Abhari, Jessica, Madhav Jivrajani, Kiran Johns, Scott Johnstun, Jonathan-Shoemaker, Vismai K, Tal Kachmann, Naoki Kanazawa, Kang-Bae, Anton Karazeev, Paul Kassebaum, Josh Kelso,

Spencer King, Knabberjoe, Yuri Kobayashi, Arseny Kovyrsin, Rajiv Krishnakumar, Vivek Krishnan, Kevin Krsulich, Prasad Kumkar, Gawel Kus, Ryan LaRose, Enrique Lacal, Raphaël Lambert, John Lapeyre, Joe Latone, Scott Lawrence, Christina Lee, Gushu Li, Dennis Liu, Peng Liu, Yunho Maeng, Kahan Majmudar, Aleksei Malyshev, Joshua Manela, Jakub Marecek, Manoel Marques, Dmitri Maslov, Dolph Mathews, Atsushi Matsuo, Douglas T. McClure, Cameron McGarry, David McKay, Dan McPherson, Srujan Meesala, Thomas Metcalfe, Martin Mevissen, Andrew Meyer, Antonio Mezzacapo, Rohit Midha, Zlatko Minev, Abby Mitchell, Nikolaj Moll, Jhon Montanez, Michael Duane Mooring, Renier Morales, Niall Moran, Mario Motta, MrF, Prakash Murali, Jan Müggenburg, David Nadlinger, Ken Nakanishi, Giacomo Nannicini, Paul Nation, Edwin Navarro, Yehuda Naveh, Scott Wyman Neagle, Patrick Neuweiler, Johan Nicander, Pradeep Niroula, Hassi Norlen, NuoWenLei, Lee James O’Riordan, Oluwatobi Ogunbayo, Pauline Ollitrault, Raul Otaolea, Steven Oud, Dan Padilha, Hanhee Paik, Soham Pal, Yuchen Pang, Simone Perriello, Anna Phan, Francesco Piro, Marco Pistoia, Christophe Piveteau, Pierre Pocreau, Alejandro Pozas-iKerstjens, Viktor Prutyantov, Daniel Puzzuoli, Jesús Pérez, Quintiii, Rafey Iqbal Rahman, Arun Raja, Nipun Ramagiri, Anirudh Rao, Rudy Raymond, Rafael Martín-Cuevas Redondo, Max Reuter, Julia Rice, Marcello La Rocca, Diego M. Rodríguez, RohithKarur, Max Rossmannek, Mingi Ryu, Tharrmashastha SAPV, SamFerracin, Martin Sandberg, Hirday Sandesara, Ritvik Sapra, Hayk Sargsyan, Aniruddha Sarkar, Ninad Sathaye, Bruno Schmitt, Chris Schnabel, Zachary Schoenfeld, Travis L. Scholten, Eddie Schoute, Joachim Schwarm, Ismael Faro Sertage, Kanav Setia, Nathan Shammah, Yunong Shi, Adenilton Silva, Andrea Simonetto, Nick Singstock, Yukio Siraichi, Iskandar Sitdikov, Seyon Sivarajah, Magnus Berg Sletfjerd, John A. Smolin, Mathias Soeken, Igor Olegovich Sokolov, Igor Sokolov, SooluThomas, Starfish, Dominik Steenken, Matt Stypulkoski, Shaojun Sun, Kevin J. Sung, Hitomi Takahashi, Tanvesh Takawale, Ivano Tavernelli, Charles Taylor, Pete Taylour, Soolu Thomas, Mathieu Tillet, Maddy Tod, Miroslav Tomasik, Enrique de la Torre, Kenso Trabing, Matthew Treinish, TrishaPe, Davindra Tulsi, Wes Turner, Yotam Vaknin, Carmen Recio Valcarce, Francois Varchon, Almudena Carrera Vazquez, Victor Villar, Desiree Vogt-Lee, Christophe Vuillot, James Weaver, Johannes Weidenfeller, Rafal Wieczorek, Jonathan A. Wildstrom, Erick Winston, Jack J. Woehr, Stefan Woerner, Ryan Woo, Christopher J. Wood, Ryan Wood, Stephen Wood, Steve Wood, James Wootton, Daniyar Yeralin, David Yonge-Mallo, Richard Young, Jessie Yu, Christopher Zachow, Laura Zdaniski, Helena Zhang, Christa Zoufal, Zoufalc, a kapila, a matsuo, bcamorrison, brandhsn, nick bronn, chlorophyll zz, dekel.meirom, dekelmeirom, dekoool, dime10, drholmie, dtrenev, ehchen, elfrocampeador, faisalde-

bouni, fanizzamarco, gabrieleagl, gadial, galeinston, georgios ts, gruu, hhorii, hykavitha, jagunther, jliu45, jscott2, kanejess, klinvill, krutik2966, kurarr, lerongil, ma5x, merav aharoni, michelle4654, ordmoj, sagar pahwa, rmoyard, saswati qiskit, scottkelso, sethmerkel, strickroman, sumitpuri, tigerjack, toural, tsura crisaldo, vvilpas, welien, willhbang, yang.luh, yotamvakninibm, and Mantas Čepulkovskis. Qiskit: An open-source framework for quantum computing, 2019.

- [36] Adam Paszke, Sam Gross, Francisco Massa, Adam Lerer, James Bradbury, Gregory Chanan, Trevor Killeen, Zeming Lin, Natalia Gimelshein, Luca Antiga, Alban Desmaison, Andreas Kopf, Edward Yang, Zachary DeVito, Martin Raison, Alykhan Tejani, Sasank Chilamkurthy, Benoit Steiner, Lu Fang, Junjie Bai, and Soumith Chintala. Pytorch: An imperative style, high-performance deep learning library. pages 8024–8035, 2019.
- [37] Diederik P Kingma and Jimmy Ba. Adam: A method for stochastic optimization. *arXiv preprint arXiv:1412.6980*, 2014.
- [38] Zihang Dai, Zhilin Yang, Fan Yang, William W Cohen, and Russ R Salakhutdinov. Good semi-supervised learning thataaa requires a bad GAN. In *Advances in neural information processing systems*, pages 6510–6520, 2017.